

# RaffeSDG: Random Frequency Filtering enabled Single-source Domain Generalization for Medical Image Segmentation

Heng Li, Haojin Li, Jianyu Chen, Huazhu Fu, Jiang Liu

**Abstract**—Deep learning models often encounter challenges in making accurate inferences when there are domain shifts between the source and target data. This issue is particularly pronounced in clinical settings due to the scarcity of annotated data resulting from the professional and private nature of medical data. Despite the existence of decent solutions, many of them are hindered in clinical settings due to limitations in data collection and computational complexity. To tackle domain shifts in data-scarce medical scenarios, we propose a *Random frequency filtering enabled Single-source Domain Generalization* algorithm (RaffeSDG), which promises robust out-of-domain inference with segmentation models trained on a single-source domain. A frequency filter-based data augmentation strategy is first proposed to promote domain variability within a single-source domain by introducing variations in frequency space and blending homologous samples. Then Gaussian filter-based structural saliency is also leveraged to learn robust representations across augmented samples, further facilitating the training of generalizable segmentation models. To validate the effectiveness of RaffeSDG, we conducted extensive experiments involving out-of-domain inference on segmentation tasks for three human tissues imaged by four diverse modalities. Through thorough investigations and comparisons, compelling evidence was observed in these experiments, demonstrating the potential and generalizability of RaffeSDG. The code is available at [https://github.com/liamheng/Non-IID\\_Medical\\_Image\\_Segmentation](https://github.com/liamheng/Non-IID_Medical_Image_Segmentation).

**Index Terms**—Single-source domain generalization, medical image segmentation, frequency filtering, data augmentation.

## I. INTRODUCTION

Deep learning-based algorithms have been widely acknowledged in numerous recent studies. However, transitioning these algorithms from controlled laboratory settings to real-world scenarios poses issues. In laboratory settings, datasets can be closed, with training (source) and test (target) data being independent and identically distributed (IID). In contrast, real-world scenarios often involve open datasets where the test data is unseen and probably non-IID with the training data [1]. This variability between training and test data is known as *domain shifts*, which detrimentally impact model performance [2].

This work was supported in part by the National Natural Science Foundation of China (82272086, 82102189), Guangdong Provincial Department of Education (SJZLGC202202). (Corresponding Author: Jiang Liu, liuj@sustech.edu.cn)

H. Li and J. Liu are with the Research Institute of Trustworthy Autonomous Systems, Southern University of Science and Technology, Shenzhen, China; H. Li, J. Chen, and J. Liu are with the Department of Computer Science and Engineering, Southern University of Science and Technology, Shenzhen, China; H. Fu is with the Institute of High Performance Computing, Agency for Science, Technology and Research, Singapore.

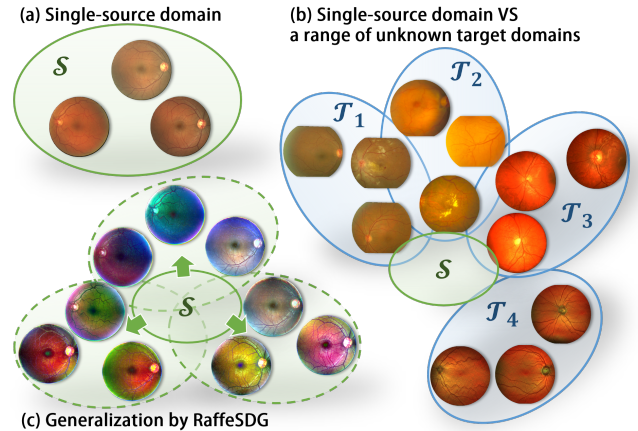


Fig. 1. Illustration of single-source domain generalization. (c) RaffeSDG enables generalization within (a) a single-source domain, allowing for inference over (b) a range of unseen target domains.

Furthermore, deep learning requires an ample amount of labeled training data [3], which involves the labor-intensive and expensive task of pixel-accurate annotations in segmentation tasks. In the case of medical images, variations in imaging modalities, acquisition protocols, or patient demographics result in diverse domain shifts, which not only contribute to a scarcity of annotated data for medical image segmentation but also exacerbate the impact on clinical inference.

To mitigate the impact of domain shifts, numerous studies have explored domain adaptation (DA) and domain generalization (DG) techniques [1]. DA focuses on learning domain-invariant representations by aligning source and target domains in a feature space. However, DA relies on the assumption that both source and target data are accessible simultaneously, which is not always feasible in practice. To overcome this limitation, DG has been introduced, enabling the learning of robust models that can generalize well to any target domain, even in the absence of target data. Nevertheless, implementing DG often necessitates the availability of multiple distinct source domains, which still introduces challenges in terms of data collection. Furthermore, regardless of whether it involves simultaneously accessing source and target data or leveraging multiple source domains, concerns about privacy preservation arise, particularly in sensitive medical scenarios. As an alternative to DA and DG, single-source domain generalization (SDG) [2] has been proposed, which focuses on a worst-

case scenario in DG involving out-of-domain inference from a single-source domain (shown in Fig. 1). By utilizing only a single-source domain, SDG circumvents data collection and transmission across different centers, mitigating data dependency and privacy concerns. Various SDG paradigms [4], [5] have been developed to generalize segmentation models from a single-source medical dataset across a range of unseen distributions.

Despite the dedicated efforts to deploy deep learning models in real-world scenarios, challenges persist in clinical segmentation tasks. i) The limited availability of annotations in clinical deployment prompts researchers to utilize existing datasets with similar characteristics, aiming to reduce the burden of annotation. However, this situation inevitably encounters domain shift issues. ii) While popular DA and DG algorithms tackle domain shifts, their reliance on additional data dependency imposes additional burdens in data collection and raises privacy concerns. iii) The utilization of complex feature operations and auxiliary generative networks in existing SDG paradigms often hinder their efficiency and versatility, thereby impeding their successful clinical deployment.

To facilitate the application of SDG, we introduce a *Random frequency filtering enabled SDG* algorithm (RaffeSDG), which mitigates the computational and network training costs. RaffeSDG employs random frequency filtering and homologous sample blending to conveniently introduce randomization within the single-source domain through data augmentation. Furthermore, RaffeSDG also incorporates Gaussian filter-based structural saliency to construct a generalizable segmentor by learning robust representations in segmentation. Three human tissues imaged by four modalities are leveraged in the experiment to demonstrate the efficacy of RaffeSDG in out-of-domain inference. Our main contributions are summarised as follows:

- An efficient SDG paradigm for medical image segmentation termed RaffeSDG is developed, to alleviate the challenges in out-of-domain inference without introducing additional data dependency and privacy concerns.
- To promote diversity within a single-source domain, frequency filter-based data augmentation is accomplished using random frequency filters and sample blending to perform domain randomization.
- Cooperating with the augmentation, a generalizable segmentor is constructed by learning robust representations across samples through Gaussian filter-based structural saliency.
- The experiment presents extensive investigations and comparisons using four medical image modalities to demonstrate the benefits and versatility of RaffeSDG in out-of-domain inference.

## II. RELATED WORK

### A. Domain adaptation and domain generalization

Domain shifts severely degrade the performance of deep learning models on cross-domain inference. Extensive efforts have been dedicated to alleviating domain shifts, which can be categorized into two approaches: DA and DG.

DA encompasses both supervised and unsupervised paradigms. In supervised DA, the focus is on few-shot adaptation where only a few labeled target samples are involved in training. Nevertheless, in medical scenarios, the scarcity of annotated data makes unsupervised DA more prevalent, which aims to align the distribution of the target domain with that of the source domain by minimizing the maximal mean variability or utilizing a domain classifier. To achieve adaptation across domains, DAMAN [6] employs a domain regularizing loss to align intermediate features between the source and target domains. CSCADA [7] achieves semi-supervised DA utilizing source data through anatomical structure discrimination. Nevertheless, accessing the target domain poses a strong requirement in practice, and both paradigms suffer from a strong coupling between the source and target domains, limiting their practicality and generalizability in clinical settings.

DG serves as an alternative pipeline to tackle domain shifts [1]. In contrast to DA, the objective of DG is to learn from multiple source domains without requiring access to target domains. This reduced reliance on target data makes DG more appreciated in medical scenarios. Recently, frequency operations have gained prominence in DG algorithms to generate diverse additional training data by domain randomization [8]. FACT [9] randomizes source domains by swapping the low-frequency component between multiple source domains. Moreover, FedDG [10] improved the augmentation by employing continuous frequency space interpolation, further enhancing the realism of the generated data. Apart from augmentation techniques, learning techniques such as feature regularization and self-supervision have gained significant popularity for imposing the learning of domain-invariant representations. To learn generalizable representations, co-teacher regularization and contrastive learning were respectively leveraged in FACT [9] and FedDG [10]. Unfortunately, the requirement for multiple distinct source domains in typical DG approaches still poses difficulties in terms of data collection and preserving privacy, especially in clinical settings.

### B. Single-source domain generalization

Due to the data collection burden and privacy concerns in medical scenarios, SDG has become increasingly significant, which involves training a deep model on a single-domain dataset and expecting it to perform well on any unseen domains.

An intuitive solution of SDG is to augment the diversity of the single-source domain. To learn a generalizable model from a single-source, uncertainty-guided model generalization [2], [11] was posed, which augments the source capacity in both input and label spaces. Subsequently, attention consistency on visual corruptions (ACVC) [12] imposed the robustness to superfluous correlations in a single-source domain to generalize visual recognition models. To facilitate the augmentation within a single-source, SLAug [13] was developed to provide both global and local augmentation. Inspired by causality, Global Intensity Non-linear augmentation (GIN) and

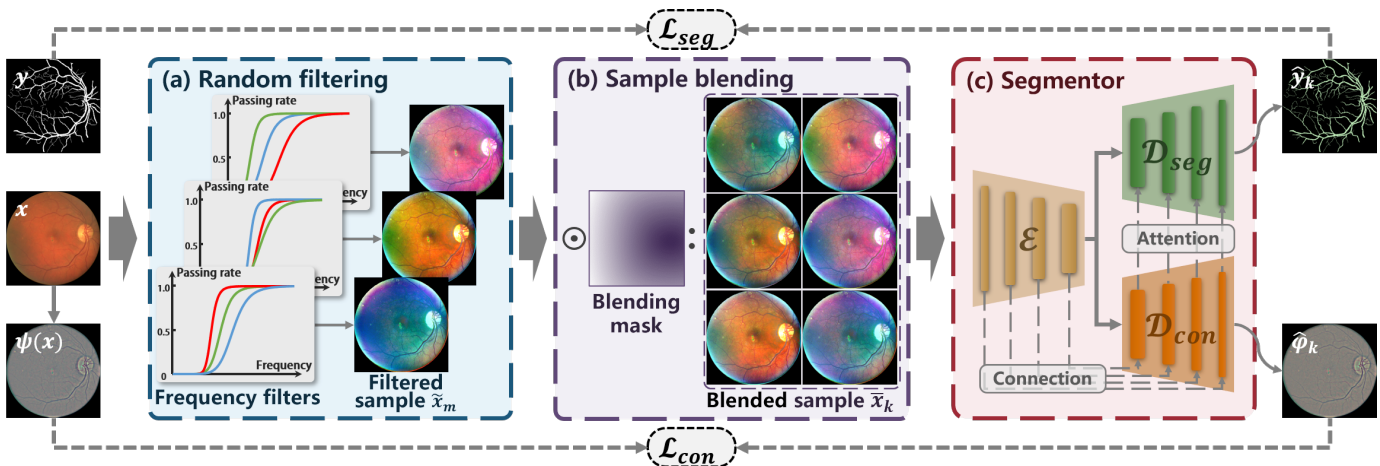


Fig. 2. Overview of RaffeSDG. Random filtering and sample blending are incorporated to introduce randomization into the single-source domain. (a) The source image  $x$  is first augmented by random high-pass frequency filters. (b) Sample blending further enables sub-image augmentation by merging filtered samples  $\tilde{x}_m$  obtained from  $x$ . (c) The segmentor integrates Gaussian filters to facilitate the learning of domain-invariant representations, and leverages attention mechanisms to appropriately forward the representations for segmentation.

Interventional Pseudocorrelation Augmentation (IPA) were devised [14] to achieve cross-domain medical image segmentation from a single-source. Furthermore, our previous study [15] has demonstrated the effectiveness of introducing domain randomization through frequency filtering, leading to the development of FreeSDG, an SDG algorithm that utilizes diverse Gaussian filters. In contrast, SDG algorithms that aim to learn invariant representations from a single-source domain have been proposed as a complementary approach to the data augmentation paradigm. Inspired by feature normalization, Semantic-Aware Normalization (SAN) and Semantic-Aware Whitening (SAW) were developed [16] to enhance the learning of domain-invariant and discriminative features.

Despite the impressive success of existing SDG algorithms, their reliance on complex feature operations or auxiliary generative networks hinders practical efficiency and versatility. To address these limitations, we have previously proposed FreeSDG [15] as a solution. However, the naive frequency operations employed in FreeSDG [15] restrict the flexibility of data augmentation (refer to Fig. 7). Therefore, RaffeSDG further incorporates random Fourier frequency filters to introduce an efficient SDG paradigm for medical image segmentation.

### III. METHOD

#### A. Definition and overview

In DG tasks, the training data from source domains are denoted as  $\mathbb{D}_S = \{(x_n^s, y_n^s)_{n=1}^{N_s}\}_{s=1}^S$ , where  $x_n^s$  refers to the  $n^{\text{th}}$  sample in the  $s^{\text{th}}$  source domain,  $y_n^s$  is the corresponding ground-truth, and  $N_s$  and  $S$  are the domain volume and the number of source domains, respectively. Based on  $\mathbb{D}_S$ , the parameters  $\theta$  of a prediction function  $g_\theta$  are learned, which maps a sample  $x$  from the image space  $\mathcal{X}$  to a label  $y$  in the label space  $\mathcal{Y}$ , i.e.,  $g_\theta : x \rightarrow y$ . The main goal of DG is to impose the learned function  $g_\theta$  generalizes well to unseen target domains  $\mathbb{D}_T = \{(x_n^t, y_n^t)_{n=1}^{N_t}\}_{t=1}^T$ , namely minimizing the error between the prediction  $\hat{y}_n^t = g_\theta(x_n^t)$  and the ground-truth  $y_n^t$ .

In pioneer studies, to ensure that  $g_\theta$  remains robust against domain shifts between  $\mathbb{D}_S$  and  $\mathbb{D}_T$ , it was common to use multiple source domains ( $S > 1$ ) for model training. More recently, to address the bottleneck in collecting multiple source domains, SDG has emerged to achieve DG in the worst-case scenario, where only one source domain ( $S = 1$ ) is available during training.

In our previous study [15], we validated the potential of frequency variations in domain randomization and successfully implemented SDG in medical image segmentation. However, the previous SDG algorithm had limitations in terms of data augmentation diversity. Therefore, we have introduced RaffeSDG in this study, which offers flexible data augmentation by utilizing random frequency filtering and homologous sample blending within the single-source domain. Subsequently, a Gaussian filter is further incorporated with RaffeSDG to boost the training of a generalizable segmentor.

#### B. Data augmentation for domain randomization

To boost the generalization and robustness of models, SDG algorithms commonly rely on data augmentation to introduce randomization within the single-source domain. As a result, previous studies have developed various data augmentation techniques, including generative networks [2], [14], [17] and visual corruption methods [12], [18]. However, the use of generative networks comes with additional computational costs and may encounter the problem of mode collapse, while visual corruption can potentially lead to the destruction of crucial structures in medical images. To overcome these limitations, we propose an effective domain randomization approach that conveniently augments data from a single-source domain using random filters and sample blending.

1) *Frequency filters based on Fourier transform:* Domain shifts can be bridged by aligning the low-level statistics between the source and target domains. Recently studies such as Fourier-based domain adaptation [19] and generalization [8], have proven that matching the low-frequency spectrum (LFS)

in image samples enables this alignment. Consequently, exchanging or integrating the LFS of one domain with another has been widely utilized to address domain shifts [9], [10].

Inspired by the Fourier-based DA and DG techniques, we hypothesize that the use of multiple source domains is not necessary for implementing domain randomization. Instead, we propose that domain randomization can be conveniently achieved by introducing random LFS variations to samples within a single-source domain. Specifically, the desired LFS variations are introduced by applying random parameters to Fourier-based high-pass filters during the frequency filtering of image samples, as exhibited in Fig. 2 (a).

For an image sample  $x(a, b)$ , it is converted into the frequency domain using Fourier transform:

$$F(u, v) = \sum_{a=0}^{M-1} \sum_{b=0}^{N-1} x(a, b) e^{-j2\pi(ua/M+vn/N)}, \quad (1)$$

where the image size is  $M \times N$ . Then a high-pass filter  $\eta(u, v)$  is applied to cut off the frequency spectrum, resulting in  $G(u, v) = F(u, v) * \eta(u, v)$ . Finally, the filtered image sample is obtained through inverse Fourier transform:

$$\tilde{x}(a, b) = \frac{1}{MN} \sum_{u=0}^{M-1} \sum_{v=0}^{N-1} G(u, v) e^{j2\pi(ua/M+vn/N)}. \quad (2)$$

Additionally, considering filters with sharp transitions can lead to the occurrence of ringing artifacts, the high-pass filter is implemented with the Butterworth filter, which is defined as

$$\eta(u, v) = \frac{1}{1 + [D_0/D(u, v)]^{2n}}, \quad (3)$$

where  $D_0$  is the cutoff frequency at which the filter starts attenuating the signal, while  $n$  is the order of the filter, influencing the steepness of the filter's roll-off.

The LFS variations can be introduced by adjusting the parameters of  $D_0$  and  $n$  (the parameter range is interpreted in Sec. IV-B). Notably, as depicted in Fig. 2 (a), distinct parameters are applied to the filter across different channels, promising the diversity of filtered samples.

To visualize the changes in data distribution resulting from the proposed filtering process, t-SNE is employed in Fig. 3. This involves dividing images from both the single-source and target domains into patches and embedding them using a pre-trained ResNet. The embedded representations are then mapped into two dimensions using t-SNE, enabling visual observation of the data distribution. From the comparison between Fig.3 (a) and (b), it can be observed that random frequency filtering expands the distribution variability within the single-source domain. This serves as evidence that LFS variations can effectively enable domain randomization.

2) *Homologous sample blending*: Although frequency filtering affects the global image, it lacks the ability to discriminatively alter local areas of the images. To overcome this limitation, we draw inspiration from popular augmentation techniques such as CutOut [20] and CutMix [21]. Consequently, homologous filtered samples are blended to introduce

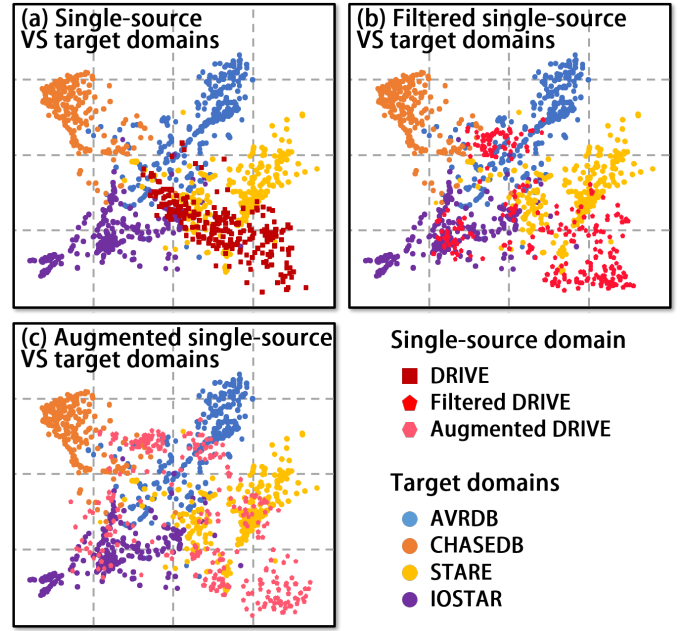


Fig. 3. Distributions of the single-source and target domains. (a) Distributions of patches from original samples in the feature space. (b) Frequency filtering extended the variability of the single-source domain. (c) Data augmentation achieved by the proposed strategy.

additional diversity at the sub-image level, effectively enhancing data augmentation.

Since the filtered samples derived from identical images inherit consistent structures, they can be seamlessly blended together. Let  $\tilde{x}_m$  and  $\tilde{x}_n$  represent two filtered samples from the image  $x$ , where  $m, n \in \mathbb{R}^N$  are the sample index and  $m \neq n$ . Then the image blending is formulated as:

$$\bar{x}_k = \Xi(\tilde{x}_m, \tilde{x}_n) = \mathcal{M} \odot \tilde{x}_m + (1 - \mathcal{M}) \odot \tilde{x}_n, \quad (4)$$

where  $\mathcal{M}$  is the blending mask and  $\odot$  is element-wise multiplication.

As shown in Fig. 2 (b), a continuous blending mask is obtained from a distance map, which is given by:

$$\mathcal{M}(a, b) = \sqrt{(a - c_w)^2 + (b - c_h)^2} / D_{Max}, \quad (5)$$

where  $(c_w, c_h)$  is the coordinates of the randomly selected distance center within the image, while  $D_{Max}$  represents the maximum distance from points in the image to the center.

Consequently, the cooperation of random frequency filtering and homologous sample blending enables sub-image level data augmentation. According to Fig. 3 (c), this augmentation approach achieves remarkable variability in the single-source domain.

### C. Generalizable segmentor using structural saliency

The data augmentation promises RaffeSDG a substantial increase in domain diversity, even within a single-source domain, facilitating the generalizability to unseen domains. Motivated by the inherent ability of the Gaussian filter to extract structural saliency, we incorporate robust representations into the segmentor of RaffeSDG to boost the robustness of representations.

The residual obtained by subtracting the Gaussian filter result from an image serves as a valuable indicator of its structural saliency [22]. Based on this insight, we incorporate a Gaussian filter within the segmentor to boost the learning of robust representations by structural saliency. For an image  $x$ , the structure saliency map  $\psi(x)$  is acquired by:

$$\psi(x) = x - x * g(r, \sigma), \quad (6)$$

where  $g$  is a Gaussian filter with the kernel of  $(r, \sigma)$ .  $r$  and  $\sigma$  are determined according to the image size following [22].

Subsequently, the structure saliency map serves as a self-supervised pretext task for the segmentor. The self-supervision loss is defined as:

$$\mathcal{L}_{sel} = \mathbb{E} \left[ \sum_{k=1}^K \|\psi(x) - \hat{\varphi}_k\|_2 \right], \quad (7)$$

where  $\hat{\varphi}_k$  refers to the structure saliency map reconstructed from  $\bar{x}_k$ .

Reconstructing the structure saliency map from augmented samples may promote domain-invariant representation learning. Therefore, to optimize the model through both self-supervision and segmentation supervision, we propose a coupling network as the segmentor, as illustrated in Fig. 2 (c). Specifically, the segmentor consists of an encoder and two decoders. The encoder  $\mathcal{E}$  processes the augmented samples  $\bar{x}_k$  and shares its outputs with both the decoder  $\mathcal{D}_{sel}$  and  $\mathcal{D}_{seg}$ , where  $\mathcal{D}_{sel}$  predicts the structure saliency and  $\mathcal{D}_{seg}$  predicts the segmentation mask.

The concrete implementation of the segmentor is outlined in Algorithm 1.  $\mathcal{E}$  is skip-connected to  $\mathcal{D}_{sel}$  to facilitate the flow of contextual information, and attention mechanisms are employed to properly integrate the self-supervision into the segmentation task. The  $l^{th}$  layer of the encoder and decoders are denoted as  $\mathcal{E}^l$ ,  $\mathcal{D}_{sel}^l$ , and  $\mathcal{D}_{seg}^l$ , with corresponding outcomes  $f_{\mathcal{E}}^l$ ,  $f_{sel}^l$ , and  $f_{seg}^l$ . The terms  $CA$  and  $SA$  represent typical channel and spatial attention respectively.

Given the segmentation objective function by:

$$\mathcal{L}_{seg} = \mathbb{E} \left[ -\sum_{c=1}^C y_k^c \log(\hat{y}_k^c) \right], \quad (8)$$

where  $\hat{y}_k$  denotes the predicted segmentation mask of  $\bar{x}_k$ , and  $c$  is the category index.

---

**Algorithm 1** Forward pass in the coupling network

---

**Require:** Augmented views  $\{\bar{x}_k | k = 1, 2, \dots, K\}$

- 1: Initialization,  $\mathcal{E}$ ,  $\mathcal{D}_{sel}$  and  $\mathcal{D}_{seg}$
  - 2:  $f_{\mathcal{E}}^L = \mathcal{E}^L(\bar{x}_k)$
  - 3: **for**  $l = L - 1, L - 2, \dots, 1$  **do**
  - 4:  $f_{\mathcal{E}}^l = \mathcal{E}^l(f_{\mathcal{E}}^{l+1})$
  - 5: **end for**
  - 6:  $f_{sel}^1 = \mathcal{D}_{sel}^1(f_{\mathcal{E}}^1)$ ,  $f_{seg}^1 = \mathcal{D}_{seg}^1(f_{\mathcal{E}}^1)$
  - 7: **for**  $l = 2, 3, \dots, L$  **do**
  - 8:  $f_{sel}^l = \mathcal{D}_{sel}^l([f_{\mathcal{E}}^{l-1}, f_{sel}^{l-1}])$
  - 9:  $f_{seg}^l = \mathcal{D}_{seg}^l([f_{sel}^{l-1}, f_{seg}^{l-1}] \otimes CA \otimes SA)$
  - 10: **end for**
  - 11:  $\hat{\varphi}_k = f_{sel}^L$ ,  $\hat{y}_k = \text{sigmoid}(f_{seg}^L)$
- 

Thus the segmentation network is optimized by the overall objective function:

$$\mathcal{L}_{total} = \mathcal{L}_{sel}(\mathcal{E}, \mathcal{D}_{sel}) + \alpha \mathcal{L}_{seg}(\mathcal{E}, \mathcal{D}_{sel}, \mathcal{D}_{seg}), \quad (9)$$

where  $\alpha$  balances  $\mathcal{L}_{consist}$  and  $\mathcal{L}_{seg}$ .

## IV. EXPERIMENTS

Out-of-domain inference experiments were conducted to demonstrate the potential of RaffeSDG. The first experiment examined the performance and settings of the proposed augmentation strategy. Then comprehensive comparisons were conducted between RaffeSDG and SOTA algorithms, including vanilla, DA, DG, and SDG segmentation methods, to present the superiority of RaffeSDG in medical image segmentation tasks. Additionally, ablation studies were performed to assess the impact of source data volume and the effectiveness of the proposed modules in RaffeSDG.

### A. Experiment settings

1) *Datasets:* The experiments utilized four medical imaging modalities obtained from three different human tissues, as summarized in Table I. The data for the vessel and retinal layer were publicly available, while the data for the joint cartilage were collected in collaboration with our partner, Southern University of Science and Technology Hospital, using discrepant ultrasound configurations of gain and grayscale. In order to generalize and assess segmentation models across these datasets, the ground-truth annotations were standardized. The datasets of DRIVE, HC-MS, and A were respectively employed as the single-source domain for each tissue, while the remaining datasets were treated as unseen target domains.

Moreover, during the comparisons, the target domains were visible to the DA algorithms, and the extensive fundus photography dataset of EyePACS was incorporated as additional source domains to implement typical DG algorithms.

2) *Implementation:* For all segmentation tasks, the input image size was set to  $512 \times 512$ , and a batch size of 2. The training data were divided into training and validation subsets in 1:1. The models were trained using the Adam optimizer. Initially, the learning rate was set to 1e-3 for the first 80 epochs. Subsequently, a linear decrease to zero was applied over the next 120 epochs. In each epoch, ten augmented samples were randomly derived from each training sample. To ensure efficient training, the early stop was implemented. During the inference, the segmentation is performed using the original images without any augmentation.

TABLE I  
EXPERIMENTAL DATA SUMMARY

| Tissue          | Modality           | Dataset                                | Volume                      |
|-----------------|--------------------|--|-----------------------------|
| Vessel          | Fundus photography | DRIVE, AVRDB, CHASEDB, STARE           | 40, 100, 28, 20             |
|                 |                    | SLO-RGB                                | IOSTAR                      |
|                 | Retinal layer      | OCT                                    | HC-MS, DUKE-AMD GOALS, AROI |
| Joint cartilage | Ultrasound         | 4 clinical datasets referred to as A~D | 1597, 956, 982, 1455        |

## B. Data augmentation configuration in RaffeSDG

We conduct an investigation into the data augmentation configuration of RaffeSDG, which encompasses the exploration of filter types and blending strategies, as well as the random range of parameters.

1) *Filter types and blending strategies*: To validate the configuration of the proposed data augmentation approach in RaffeSDG, we explored different filter types and blending strategies. The filtered and blended samples are illustrated in Fig. 4. Moreover, training data is augmented from DRIVE, and a vanilla U-Net is trained to quantitatively evaluate the performance of various configurations on the target domains, as summarized in Table II.

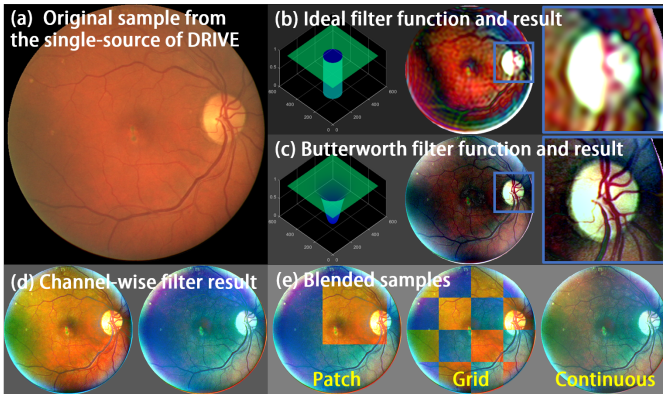


Fig. 4. Frequency-filtered images. (a) Original image. (b) Function diagram and filtered result using an ideal filter. (c) Function diagram and filtered image using a Butterworth filter. (d) Filtered images using channel-wise Butterworth filters. (e) Samples blended from filtered ones.

**Filter type**: To analyze the impact of filter types on data augmentation, we employ both the ideal filter and the Butterworth filter to introduce variations into the LFS of images. Fig.4 (b) presents the function diagram and the filtered result of the ideal filter. The sharp cutoff frequency of the ideal filter leads to the presence of ringing artifacts in the filtered result. On the other hand, the Butterworth filter offers a smoother transition between the passband and stopband, reducing the occurrence of ringing artifacts. Thus, the Butterworth filter is deemed more suitable for data augmentation, as illustrated in Fig.4 (c). Additionally, to enhance diversity in the augmented samples, we implement a channel-wise filter by applying Butterworth filters with different parameters to the RGB channels, as depicted in Fig. 4 (d). Consequently, superior performance is achieved by the channel-wise filter in Table II.

**Blending strategy**: To interpret the effect of blending, we compare three strategies, including patch, grid, and continuous mask, as illustrated in Fig.4 (e). The images blended using patch and grid masks exhibit a noticeable gap, which deviates from real-world scenarios and hampers the overall context. In contrast, the continuous mask enables a seamless context in the augmented image, resulting in a more coherent representation that aligns well with real-world scenarios. The evaluation results provided in Table II further validate our choice of filter and blending configurations. Accordingly, the channel-wise

TABLE II  
AUGMENTATION CONFIGURATION COMPARISON ON TRAINING U-NET USING ONLY DRIVE FOR OUT-OF-DOMAIN SEGMENTATION.

| Configuration       | DICE         |              |              |              | Avg.         |
|---------------------|--------------|--------------|--------------|--------------|--------------|
|                     | AVRDB        | CHASEDB      | STARE        | IOSTAR       |              |
| U-Net only          | 0.549        | 0.219        | 0.600        | 0.594        | 0.491        |
| Ideal filter        | 0.333        | 0.365        | 0.425        | 0.540        | 0.416        |
| Butterworth filter  | 0.510        | 0.411        | 0.602        | 0.670        | 0.548        |
| Channel-wise filter | <b>0.570</b> | <b>0.583</b> | <b>0.671</b> | <b>0.701</b> | <b>0.631</b> |
| Patch mask          | 0.586        | 0.591        | 0.692        | 0.706        | 0.639        |
| Grid mask           | 0.580        | 0.586        | 0.685        | 0.703        | 0.646        |
| Continuous mask     | <b>0.593</b> | <b>0.691</b> | <b>0.699</b> | <b>0.720</b> | <b>0.676</b> |

filter and the continuous mask are cooperated to implement RaffeSDG.

2) *Parameter range*: According to Eq. 3, the Butterworth filter is controlled by two parameters,  $D_0$  and  $n$ .  $D_0$  determines the frequency at which the filter starts attenuating the signal, while  $n$  determines the steepness of the filter's roll-off. Fig. 5 illustrates the impact of varying  $D_0$  and  $n$  on the Butterworth filter's behavior.

As shown in Fig. 5,  $n$  has a minor influence on the filtered results, while increasing the value of  $D_0$  leads to a reduction in the low-frequency style and an increase in the visibility of artifacts. However, using high values for both  $n$  and  $D_0$  can aggravate the appearance of ringing artifacts. Based on these observations, we have determined that setting the parameter range as  $D_0 \leq 0.04r$  ( $r$  is the radius of the spectrum of an image) and  $n \leq 3$  to provide satisfactory results and mitigate the risk of unwanted artifacts.

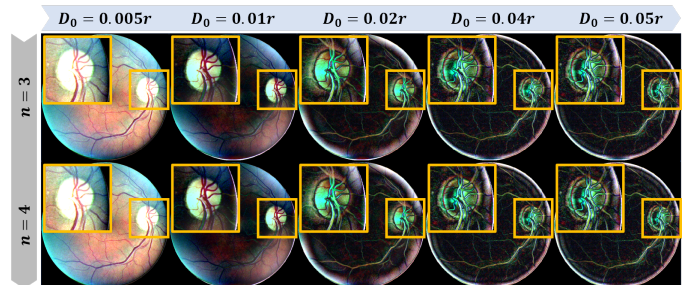


Fig. 5. Filtering results with varying  $D_0$  and  $n$ , where  $r$  represents the radius of the spectrum of an image.

## C. Augmentation comparison

Considering the expansion of the single-source domain plays a crucial role in achieving SDG, a comparison focusing on augmentation performance is conducted to validate the benefit of the proposed augmentation in RaffeSDG.

The comparison includes both commonly used augmentation techniques and augmentation approaches designed in SDG algorithms. Specifically, the augmentation techniques include geometric transformation, CutOut [20], and CutMix [21]. And the SDG augmentation approaches are collected from ACVC [12], SLAug [13], GIN-IPA [14], and FreeSDG [15]. In the comparison, the dataset of DRIVE is utilized as the single-source domain, and a vanilla U-Net serves as the unified segmentor, which is trained with augmented data and

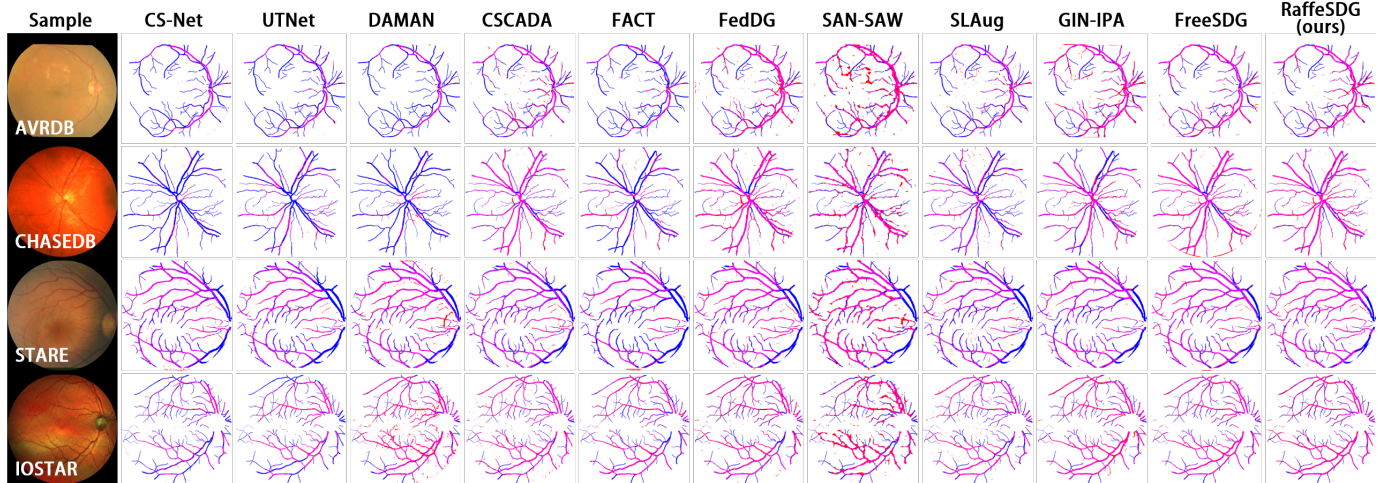


Fig. 6. Visualized comparison of out-of-domain inferences among SOTA segmentation algorithms. The **ground-truth masks** are represented in blue, the **predictions** made by the algorithms are represented in red, and the **correctly identified pixels** are represented in magenta.

conducts out-of-domain inference. The augmented samples are visualized in Fig. 7, while the segmentation performance is quantified in Table III by training a U-Net.

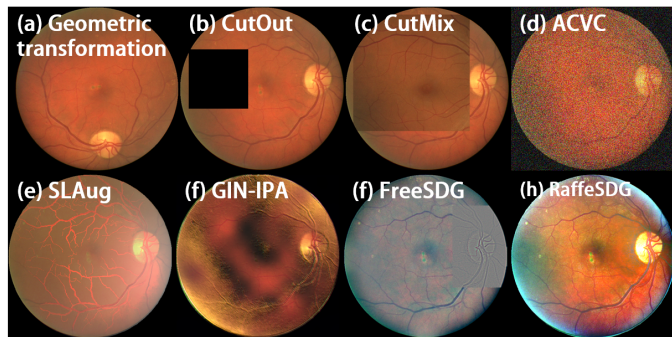


Fig. 7. Samples augmented by various augmentation techniques.

As depicted in Fig. 7, the native augmentation strategy of geometric transformation, CutOut [20], and CutMix [21] are constrained to the single-source domain, leading to limited appearance variations in the augmented samples. In contrast, the augmentation approaches used in SDG tasks present remarkable performance in Table III. For implementing SDG in classification, ACVC [12] introduces 19 visual corruptions and 3 Fourier-based corruptions to augment the single-source domain. For medical image segmentation, SLAug [13] introduces a saliency-balancing fusion strategy that combines global-scale and local location-scale aspects to augment the single-source domain. Moreover, GIN-IPA [14] proposes a causality-inspired data augmentation approach, which utilizes global intensity non-linear augmentation to diversify the appearances of medical images and addresses confounders through interventional pseudo-correlation augmentation.

In our previous study, FreeSDG [15] utilized Gaussian filters to introduce LFS variations into samples, and combined with patch masks to merge the filtered results. However, although randomization was introduced through the augmentation of FreeSDG [15], the single-source domain, limited diversity was

TABLE III  
AUGMENTATION TECHNIQUE COMPARISON ON TRAINING U-NET. THE TOP THREE RESULTS ARE INDICATED IN **RED**, **MAGENTA**, AND **BLUE**.

| Augmentation   | DICE         |              |              |              |              |
|----------------|--------------|--------------|--------------|--------------|--------------|
|                | AVRDB        | CHASEDB      | STARE        | IOSTAR       | Avg.         |
| Geometric      | 0.549        | 0.219        | 0.600        | 0.594        | 0.491        |
| CutOut [20]    | 0.502        | 0.189        | 0.606        | 0.411        | 0.427        |
| CutMix [21]    | 0.569        | 0.390        | 0.609        | 0.665        | 0.558        |
| ACVC [12]      | <b>0.609</b> | 0.613        | <b>0.727</b> | <b>0.701</b> | <b>0.663</b> |
| SLAug [13]     | 0.569        | 0.580        | 0.635        | 0.646        | 0.608        |
| GIN-IPA [14]   | 0.580        | <b>0.647</b> | 0.674        | <b>0.694</b> | 0.649        |
| FreeSDG [15]   | <b>0.632</b> | <b>0.671</b> | <b>0.677</b> | 0.690        | <b>0.668</b> |
| FreeAug (ours) | <b>0.593</b> | <b>0.691</b> | <b>0.699</b> | <b>0.720</b> | <b>0.676</b> |

observed in Fig. 7 (f), resulting in suboptimal performance as indicated in Table III. Fortunately, the augmentation approach proposed in RaffeSDG successfully introduces a wide range of visual variations in the single-source domain, as illustrated in Fig. 7 (h). This diversification strategy has proven to be effective, surpassing alternative methods in training the U-Net model and achieving superior performance, as demonstrated in Table III.

#### D. Comparison with segmentation algorithms

Comparisons with SOTA segmentation and SDG algorithms are conducted to validate the advantages of the proposed RaffeSDG. The visualized results are presented in Fig. 6, while quantitative evaluations are summarized in Table IV and V.

1) *Comparison with segmentation algorithms:* We employ 6 SOTA segmentation algorithms as baselines. Specifically, CS-Net [23] and UINet [24] are utilized, which are vanilla segmentation algorithms for medical images trained solely on the training data. For domain adaptive segmentation algorithms, DAMAN [6] and CSCADA [7] are implemented, which are trained using both the training data and unlabeled test data. Additionally, FACT [9] and FedDG [10] are also included, which are segmentation algorithms based on domain generalization trained with multiple source domains.

TABLE IV  
COMPARISON WITH SOTA SEGMENTATION ALGORITHMS. THE TOP THREE RESULTS ARE INDICATED IN RED, MAGENTA, AND BLUE.

| Algorithms      | Dependency* |    | DICE         |              |              |              |              | IoU          |              |              |              |              |
|-----------------|-------------|----|--------------|--------------|--------------|--------------|--------------|--------------|--------------|--------------|--------------|--------------|
|                 | VT          | MS | AVRDB        | CHASEDB      | STARE        | IOSTAR       | Avg.         | AVRDB        | CHASEDB      | STARE        | IOSTAR       | Avg.         |
| CS-Net [23]     | /           | /  | 0.576        | 0.233        | 0.580        | 0.576        | 0.491        | 0.324        | 0.132        | 0.408        | 0.405        | 0.317        |
| UTNet [24]      | /           | /  | 0.527        | 0.410        | 0.661        | 0.614        | 0.553        | 0.357        | 0.258        | 0.493        | 0.443        | 0.388        |
| DAMAN [6]       | *           |    | 0.508        | 0.395        | 0.689        | 0.682        | 0.569        | 0.341        | 0.228        | 0.519        | 0.517        | 0.401        |
| CSCADA [7]      | *           |    | <b>0.630</b> | <b>0.694</b> | <b>0.703</b> | <b>0.741</b> | <b>0.692</b> | <b>0.460</b> | <b>0.531</b> | <b>0.542</b> | <b>0.588</b> | <b>0.530</b> |
| FACT [9]        |             | *  | 0.581        | 0.480        | 0.561        | 0.661        | 0.571        | 0.409        | 0.325        | 0.390        | 0.493        | 0.404        |
| FedDG [10]      |             | *  | <b>0.663</b> | <b>0.659</b> | <b>0.752</b> | <b>0.697</b> | <b>0.693</b> | <b>0.496</b> | <b>0.492</b> | <b>0.602</b> | <b>0.535</b> | <b>0.531</b> |
| RaffeSDG (ours) |             |    | <b>0.661</b> | <b>0.731</b> | <b>0.775</b> | <b>0.749</b> | <b>0.729</b> | <b>0.493</b> | <b>0.576</b> | <b>0.633</b> | <b>0.599</b> | <b>0.575</b> |

\* Dependency on visiting test data (VT) and multiple source domains (MS) are indicated by \*.

TABLE V  
COMPARISON WITH SDG ALGORITHMS.

| SDG algorithms  | DICE         |              |              |              |              | IoU          |              |              |              |              |
|-----------------|--------------|--------------|--------------|--------------|--------------|--------------|--------------|--------------|--------------|--------------|
|                 | AVRDB        | CHASEDB      | STARE        | IOSTAR       | Avg.         | AVRDB        | CHASEDB      | STARE        | IOSTAR       | Avg.         |
| SAN-SAW [16]    | 0.582        | 0.560        | 0.584        | 0.531        | 0.564        | 0.410        | 0.389        | 0.412        | 0.361        | 0.393        |
| SLAug [13]      | 0.626        | <b>0.662</b> | <b>0.717</b> | 0.683        | 0.672        | 0.456        | <b>0.495</b> | <b>0.559</b> | 0.519        | 0.507        |
| GIN-IPA [14]*   | <b>0.649</b> | 0.654        | 0.712        | <b>0.717</b> | <b>0.683</b> | <b>0.481</b> | 0.486        | 0.553        | <b>0.559</b> | <b>0.520</b> |
| FreeSDG [15]    | <b>0.669</b> | <b>0.696</b> | <b>0.732</b> | <b>0.736</b> | <b>0.708</b> | <b>0.503</b> | <b>0.533</b> | <b>0.578</b> | <b>0.582</b> | <b>0.549</b> |
| RaffeSDG (ours) | <b>0.661</b> | <b>0.731</b> | <b>0.775</b> | <b>0.749</b> | <b>0.729</b> | <b>0.493</b> | <b>0.576</b> | <b>0.633</b> | <b>0.599</b> | <b>0.575</b> |

\* A few cases of failure to converge were also observed, due to model collapse.

The comparative algorithms are trained based on their data dependency, with the DRIVE dataset serving as the default training data. The segmentation results are summarized in Table IV. Due to the lack of specific design for handling domain shifts, CS-Net [23] and UTNet [24] trained on the DRIVE dataset experience a notable decline in performance when applied to other datasets. By incorporating unlabeled test data during model training, DAMAN [6] and CSCADA [7] bridge domain shifts, resulting in improved performance in the target domains. Furthermore, FACT [9] and FedDG [10] utilize multiple source domains to learn generalizable segmentation models, demonstrating decent performance on unseen target domains.

Despite relying solely on the single-source domain of DRIVE without any additional data, the proposed RaffeSDG effectively learns generalizable segmentation models, leading to superior performance on newly encountered datasets.

2) *Comparison with SDG algorithms*: Four SDG algorithms, including SAN-SAW [16], SLAug [13], GIN-IPA [14], and FreeSDG [15] are also compared and summarized in Table V.

SAN-SAW [16] incorporates normalization and whitening to learn domain-invariant and discriminative features, it faces challenges in effectively handling fine vessel structures. Consequently, SAN-SAW [16] exhibits false positive segmentation in Fig.6. SLAug [13] introduces a saliency-balancing fusion strategy for data augmentation, improving the out-of-domain segmentation based on the single-source domain. Meanwhile, GIN-IPA [14] employs global intensity non-linear augmentation to diversify appearances and interventional pseudo-correlation augmentation to address confounders. Though SLAug [13] and GIN-IPA [14] demonstrate impressive performance, the use of auxiliary generative networks increases the risk of model collapse.

By incorporating frequency variations and employing a jointly supervised segmentor, both FreeSDG [15] and RaffeSDG demonstrate exceptional performance compared

to other SDG paradigms. They also offer the advantage of convenient implementation, eliminating the need for intricate calculations and generative network tuning. However, due to the limited diversity of frequency variations using Gaussian filters, FreeSDG [15] exhibits suboptimal performance when compared to RaffeSDG. In contrast, RaffeSDG introduces more flexible frequency variation and image blending strategies, enabling robust randomization within the single-source domain. This leads to superior performance in out-of-domain segmentation tasks.

### E. Ablation studies

1) *Data volume impact*: To gain a comprehensive understanding of the potential of RaffeSDG, we conducted an analysis to assess the influence of data volume from a single-source. Specifically, we progressively increased the number of raw samples from DRIVE to examine its impact on the generalization performance of the model developed by RaffeSDG. It is worth noting that throughout the study, we maintained a consistent volume of augmented training data by randomly augmenting additional samples.

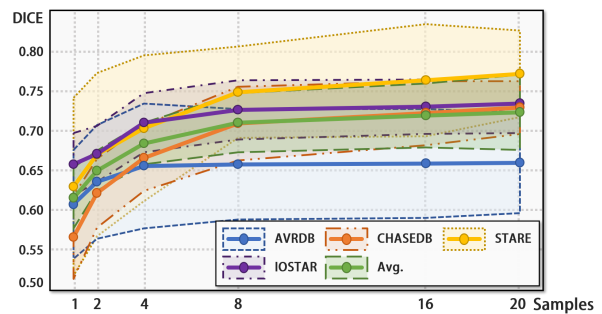


Fig. 8. The segmentation performance on out-of-domain data impacted by the data volume from a single-source. The mean and variance of the predictions on unseen target domains are exhibited.

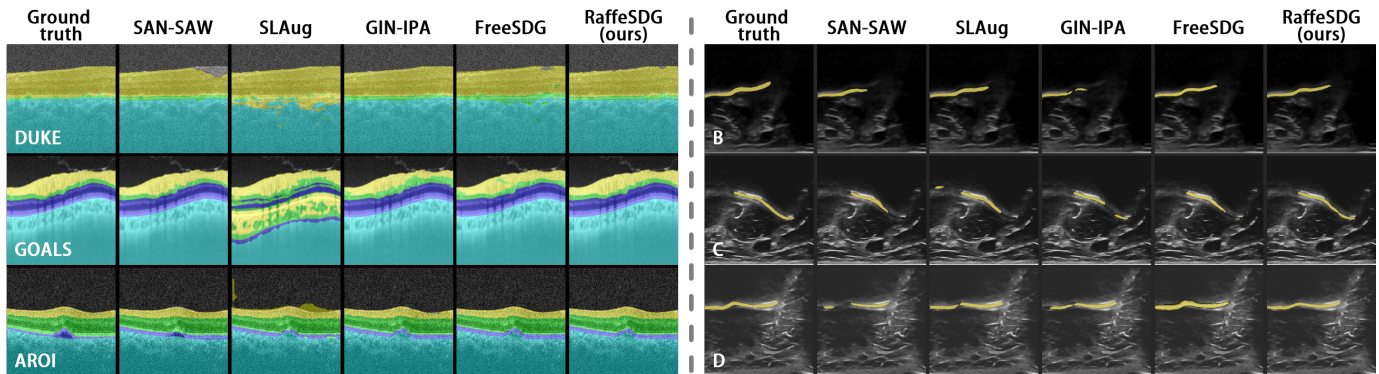


Fig. 9. Visualized comparisons with SOTA SDG algorithms for OCT and ultrasound segmentation.

TABLE VI  
COMPARISONS OF OCT AND ULTRASOUND SEGMENTATION. THE TOP THREE RESULTS ARE INDICATED IN RED, MAGENTA, AND BLUE.

| SDG algorithms | OCT DICE     |              |              |              | Ultrasound DICE |              |              |              |
|----------------|--------------|--------------|--------------|--------------|-----------------|--------------|--------------|--------------|
|                | DUKE         | GOALS        | AROI         | Avg.         | B               | C            | D            | Avg.         |
| SAN-SAW [16]   | 0.860        | <b>0.613</b> | <b>0.771</b> | <b>0.748</b> | 0.735           | 0.825        | 0.750        | 0.770        |
| SLAug [13]     | 0.483        | 0.316        | 0.458        | 0.419        | <b>0.745</b>    | 0.830        | <b>0.765</b> | <b>0.780</b> |
| GIN-IPa [14]   | <b>0.952</b> | <b>0.569</b> | 0.703        | <b>0.743</b> | 0.715           | <b>0.834</b> | <b>0.781</b> | 0.777        |
| FreeSDG [15]   | <b>0.885</b> | 0.565        | <b>0.760</b> | 0.736        | <b>0.750</b>    | <b>0.826</b> | 0.759        | <b>0.778</b> |
| RaffeSDG(ours) | <b>0.901</b> | <b>0.579</b> | <b>0.778</b> | <b>0.753</b> | <b>0.766</b>    | <b>0.847</b> | <b>0.793</b> | <b>0.802</b> |

The performance achieved by different volumes of raw single-source samples is presented in Fig. 8. Notable impacts can be observed when the data volume is relatively small (sample size less than 8), as the out-of-domain performance demonstrates significant improvement with increasing sample size. However, as the sample size reaches 8, convergence begins to occur, and the rate of performance improvement gradually becomes limited with further increases in sample size. Furthermore, even with only one raw sample, RaffeSDG allows an average performance of  $0.616 \pm 0.038$  in DICE across all target domains, surpassing the performance of several existing SOTA algorithms.

This indicates that RaffeSDG effectively alleviates the burden of extensive data collection, and it consistently delivers strong performance even in few-shot conditions.

2) *Ablation against segmentor modules*: The effectiveness of the modules in the segmentor of RaffeSDG is verified through ablation studies, as summarized in Figure 10. To begin the study, a benchmark is established using only the U-Net backbone to make predictions in unseen target domains from the single-source of DRIVE. Subsequently, to enhance the diversity of the single-source domain, data augmentation is introduced using the proposed strategy. Furthermore, the Gaussian-filter-based self-supervision is incorporated to facilitate the learning of domain-invariant representations. Lastly, attention blocks are implemented to improve the utilization of representations from the pretext task in the segmentation task.

As observed in Fig. 10, the introduction of data augmentation significantly enhances out-of-domain segmentation by the backbone module. Then, the self-supervision based on Gaussian filters imposes additional constraints across augmented samples, enabling the learning of domain-invariant representations within the segmentor. Afterward, the attention blocks efficiently incorporate the representations learned from

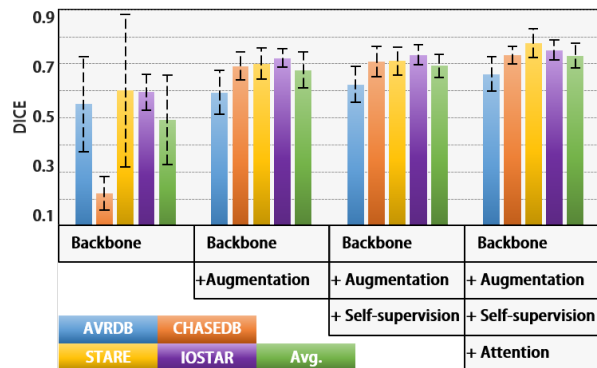


Fig. 10. Ablation study of the proposed modules in RaffeSDG.

the pretext tasks, resulting in a significant enhancement in out-of-domain inference capabilities of the segmentor.

### F. Versatility for various tissues and imaging modalities

Comparisons of out-of-domain inference for OCT and ultrasound image segmentation were also performed to validate the effectiveness of RaffeSDG. Visualized and quantitative summaries of these comparisons are respectively presented in Fig. 9 and Table VI.

Considering that SAN-SAW [16] and GIN-IPa [14] employ specific designs for multi-category labels, it is understandable that they achieve remarkable performance in the retina layer segmentation of OCT, as expressed in Table VI. However, the nature of OCT and ultrasound data poses limitations for RaffeSDG. Unlike colorful fundus data obtained through visible light, OCT and ultrasound utilize wave propagation characteristics to capture images of internal structures, resulting in an inherently grayscale appearance. Consequently, OCT

and ultrasound do not lend themselves well to the advantages of RaffeSDG, as illustrated in Fig. 9. Fortunately, despite these constraints, RaffeSDG still manages to achieve decent results, highlighting its versatility in medical image segmentation.

## V. DISCUSSIONS

The scarcity of annotated data is a common challenge in medical scenarios, leading to inevitable domain shifts in clinical settings. Furthermore, the burdens associated with data collection and computational complexity impede the practicality of many solutions. Fortunately, SDG focuses on a worst-case scenario of generalization involving out-of-domain inference from a single-source domain, offering an alternative solution to domain shifts.

RaffeSDG presents an efficient SDG paradigm by incorporating variations in frequency space and image blending. Through comparisons with common data augmentation techniques, the efficacy of the augmentation strategy devised in RaffeSDG is demonstrated. Furthermore, an exploration of optimal configurations is conducted to determine the most effective settings. Subsequently, the superior performance of RaffeSDG is showcased in comparisons with SOTA algorithms, including DA, DG, and SDG methods, in segmentation tasks involving three human tissues captured by four imaging modalities. Afterward, through ablation studies, the robustness of RaffeSDG in few-shot scenarios is demonstrated, and the effectiveness of the proposed modules is verified.

Moreover, attributed to the absence of category-wise generalization modules, the multi-category annotations in OCT retina layer segmentation have revealed certain limitations of RaffeSDG. As a result, future revisions will be pursued to incorporate multi-category annotations and address these limitations accordingly.

## VI. CONCLUSIONS

Domain shifts detrimentally impact deep learning model performance, and the scarcity of annotated data exacerbates the impact of domain shifts in medical scenarios. Despite considerable efforts to tackle these challenges, practical implementation in clinical settings is still hindered by limitations in data collection and computational complexity. To overcome these obstacles, we proposed RaffeSDG, which utilizes frequency variations to impose robust out-of-domain inference based on a single-source domain. Extensive experiments were executed to interpret the advantages and effectiveness of RaffeSDG. The efficient frequency operations endow RaffeSDG with superiority and efficiency in segmenting out-of-domain data, even when faced with limited training data.

## REFERENCES

- [1] K. Zhou, Z. Liu, Y. Qiao, T. Xiang, and C. C. Loy, "Domain generalization: A survey," *IEEE Transactions on Pattern Analysis and Machine Intelligence*, 2022.
- [2] X. Peng, F. Qiao, and L. Zhao, "Out-of-domain generalization from a single source: An uncertainty quantification approach," *IEEE Transactions on Pattern Analysis and Machine Intelligence*, 2022.
- [3] H. Jiang, M. Gao, H. Li, R. Jin, H. Miao, and J. Liu, "Multi-learner based deep meta-learning for few-shot medical image classification," *IEEE Journal of Biomedical and Health Informatics*, vol. 27, no. 1, pp. 17–28, 2022.
- [4] X. Liu, S. Thermos, P. Sanchez, A. Q. O’Neil, and S. A. Tsaftaris, "vmfnet: Compositionality meets domain-generalised segmentation," in *MICCAI*. Springer, 2022, pp. 704–714.
- [5] Z. Zhou, L. Qi, X. Yang, D. Ni, and Y. Shi, "Generalizable cross-modality medical image segmentation via style augmentation and dual normalization," in *Proceedings of the IEEE/CVF Conference on Computer Vision and Pattern Recognition*, 2022, pp. 20 856–20 865.
- [6] S. Mukherjee, R. Sarkar, M. Manich, E. Labruyere, and J.-C. Olivo-Marin, "Domain adapted multitask learning for segmenting amoeboid cells in microscopy," *IEEE Transactions on Medical Imaging*, vol. 42, no. 1, pp. 42–54, 2022.
- [7] R. Gu, J. Zhang, G. Wang, W. Lei, T. Song, X. Zhang, K. Li, and S. Zhang, "Contrastive semi-supervised learning for domain adaptive segmentation across similar anatomical structures," *IEEE Transactions on Medical Imaging*, vol. 42, no. 1, pp. 245–256, 2022.
- [8] J. Huang, D. Guan, A. Xiao, and S. Lu, "Fsd: Frequency space domain randomization for domain generalization," in *Proceedings of the IEEE/CVF Conference on Computer Vision and Pattern Recognition*, 2021, pp. 6891–6902.
- [9] Q. Xu, R. Zhang, Y. Zhang, Y. Wang, and Q. Tian, "A fourier-based framework for domain generalization," in *Proceedings of the IEEE/CVF Conference on Computer Vision and Pattern Recognition*, 2021, pp. 14 383–14 392.
- [10] Q. Liu, C. Chen, J. Qin, Q. Dou, and P.-A. Heng, "Feddg: Federated domain generalization on medical image segmentation via episodic learning in continuous frequency space," in *Proceedings of the IEEE/CVF Conference on Computer Vision and Pattern Recognition*, 2021, pp. 1013–1023.
- [11] F. Qiao and X. Peng, "Uncertainty-guided model generalization to unseen domains," in *Proceedings of the IEEE/CVF conference on computer vision and pattern recognition*, 2021, pp. 6790–6800.
- [12] I. Cugu, M. Mancini, Y. Chen, and Z. Akata, "Attention consistency on visual corruptions for single-source domain generalization," in *Proceedings of the IEEE/CVF Conference on Computer Vision and Pattern Recognition*, 2022, pp. 4165–4174.
- [13] Z. Su, K. Yao, X. Yang, K. Huang, Q. Wang, and J. Sun, "Rethinking data augmentation for single-source domain generalization in medical image segmentation," in *Proceedings of the AAAI Conference on Artificial Intelligence*, vol. 37, no. 2, 2023, pp. 2366–2374.
- [14] C. Ouyang, C. Chen, S. Li, Z. Li, C. Qin, W. Bai, and D. Rueckert, "Causality-inspired single-source domain generalization for medical image segmentation," *IEEE Transactions on Medical Imaging*, 2022.
- [15] H. Li, H. Li, W. Zhao, H. Fu, X. Su, Y. Hu, and J. Liu, "Frequency-mixed single-source domain generalization for medical image segmentation," in *International Conference on Medical Image Computing and Computer-Assisted Intervention*. Springer, 2023, pp. 127–136.
- [16] D. Peng, Y. Lei, M. Hayat, Y. Guo, and W. Li, "Semantic-aware domain generalized segmentation," in *Proceedings of the IEEE/CVF Conference on Computer Vision and Pattern Recognition*, 2022, pp. 2594–2605.
- [17] Z. Wang, Y. Luo, R. Qiu, Z. Huang, and M. Baktashmotlagh, "Learning to diversify for single domain generalization," in *Proceedings of the IEEE/CVF International Conference on Computer Vision*, 2021, pp. 834–843.
- [18] T. Duboudin, E. Dellandréa, C. Abgrall, G. Hénaff, and L. Chen, "Encouraging intra-class diversity through a reverse contrastive loss for single-source domain generalization," in *Proceedings of the IEEE/CVF International Conference on Computer Vision*, 2021, pp. 51–60.
- [19] Y. Yang and S. Soatto, "Fda: Fourier domain adaptation for semantic segmentation," in *Proceedings of the IEEE/CVF Conference on Computer Vision and Pattern Recognition*, 2020, pp. 4085–4095.
- [20] T. DeVries and G. W. Taylor, "Improved regularization of convolutional neural networks with cutout," *arXiv preprint arXiv:1708.04552*, 2017.
- [21] S. Yun, D. Han, S. J. Oh, S. Chun, J. Choe, and Y. Yoo, "Cutmix: Regularization strategy to train strong classifiers with localizable features," in *Proceedings of the IEEE/CVF international conference on computer vision*, 2019, pp. 6023–6032.
- [22] H. Li, H. Liu, Y. Hu, H. Fu, Y. Zhao, H. Miao, and J. Liu, "An annotation-free restoration network for cataractous fundus images," *IEEE Transactions on Medical Imaging*, 2022.
- [23] L. Mou, Y. Zhao, L. Chen, J. Cheng, Z. Gu, H. Hao, H. Qi, Y. Zheng, A. Frangi, and J. Liu, "Cs-net: channel and spatial attention network for curvilinear structure segmentation," in *MICCAI*. Springer, 2019, pp. 721–730.
- [24] Y. Gao, M. Zhou, and D. N. Metaxas, "Utnet: a hybrid transformer architecture for medical image segmentation," in *MICCAI*. Springer, 2021, pp. 61–71.